Journal of Biomechanics 42 (2009) 2697–2701

Contents lists available at ScienceDirect

Journal of Biomechanics

journal homepage: www.elsevier.com/locate/jbiomech
www.JBiomech.com

Regional stiffening of the mitral valve anterior leaflet in the beating ovine heart

Gaurav Krishnamurthy [a,b], Akinobu Itoh [a], Julia C. Swanson [a], Wolfgang Bothe [a], Matts Karlsson [c], Ellen Kuhl [b], D. Craig Miller [a], Neil B. Ingels Jr.[a,d,*]

[a] Department of Cardiothoracic Surgery, Stanford University School of Medicine, Stanford, CA, USA
[b] Department of Mechanical Engineering, Stanford University, Stanford, CA, USA
[c] Department of Management and Engineering, Linköping University, Linköping, Sweden
[d] Laboratory of Cardiovascular Physiology and Biophysics, Research Institute of the Palo Alto Medical Foundation, (AMES Building) 795 El Camino Real, Palo Alto, CA 94301-2302, USA

ARTICLE INFO

Article history:
Accepted 14 August 2009

Keywords:
Mitral valve
Finite element analysis
Heterogeneity
Anisotropy
Elastic modulus

ABSTRACT

Left atrial muscle extends into the proximal third of the mitral valve (MV) anterior leaflet and transient tensing of this muscle has been proposed as a mechanism aiding valve closure. If such tensing occurs, regional stiffness in the proximal anterior mitral leaflet will be greater during isovolumic contraction (IVC) than isovolumic relaxation (IVR) and this regional stiffness difference will be selectively abolished by β-receptor blockade. We tested this hypothesis in the beating ovine heart. Radiopaque markers were sewn around the MV annulus and on the anterior MV leaflet in 10 sheep hearts. Four-dimensional marker coordinates were obtained from biplane videofluoroscopy before (CRTL) and after administration of esmolol (ESML). Heterogeneous finite element models of each anterior leaflet were developed using marker coordinates over matched pressures during IVC and IVR for CRTL and ESML. Leaflet displacements were simulated using measured left ventricular and atrial pressures and a response function was computed as the difference between simulated and measured displacements. Circumferential and radial elastic moduli for ANNULAR, BELLY and EDGE leaflet regions were iteratively varied until the response function reached a minimum. The stiffness values at this minimum were interpreted as the *in vivo* regional material properties of the anterior leaflet. For all regions and all CTRL beats IVC stiffness was 40–58% greater than IVR stiffness. ESML reduced ANNULAR IVC stiffness to ANNULAR IVR stiffness values. These results strongly implicate transient tensing of leaflet atrial muscle during IVC as the basis of the ANNULAR IVC–IVR stiffness difference.

1. Introduction

Mitral valve leaflets, traditionally viewed as passive flaps, have recently been shown to exhibit active leaflet stiffening during the cardiac cycle in the beating ovine heart (Itoh et al., 2009). During each beat, the anterior leaflet is globally stiffer during isovolumic contraction (IVC) than isovolumic relaxation (IVR). We postulated that this stiffness increase during IVC was most likely due to transient tensing of the atrial cardiac muscle present in the atrialis layer of the anterior leaflet (Cooper et al., 1966; Montiel, 1970; Fenoglio et al., 1972; Hibbs and Ellison, 1973; Wit et al., 1973, 1979; Boucek et al., 1978), in the ANNULAR third of the leaflet proximal to the mitral annulus. β-receptor blockade by intravenous esmolol was found to abolish this global IVC–IVR stiffness difference. We postulated that this was due to selective decrease of IVC force development by the ANNULAR leaflet cardiac muscle (Itoh et al., 2009). Here, we analyze the data from the ten hearts in our previous study (Itoh et al., 2009) using a novel, regionally heterogeneous, inverse finite element approach to test the hypothesis that both the global IVC–IVR stiffening difference and the abolishment of this difference with β-blockade observed in our previous study, results primarily from a selective local reduction in ANNULAR IVC stiffness, i.e., in the leaflet region containing atrial cardiac muscle, rather than a uniform global effect experienced throughout the entire leaflet.

2. Methods

2.1. Data acquisition

Data acquisition methods were discussed in detail in our previous report (Itoh et al., 2009), thus will only be summarized here. Thirteen radiopaque markers were surgically implanted to silhouette the LV chamber in each heart (“Ventricular Markers”, Fig. 1a), one marker at the tip of each papillary muscle (APM, PPM, Fig.

* Corresponding author at: Laboratory of Cardiovascular Physiology and Biophysics, Research Institute of the Palo Alto Medical Foundation, (AMES Building) 795 El Camino Real, Palo Alto, CA 94301-2302, USA. Tel.: +1 650 853 4834; fax: +1 650 324 2665.
E-mail address: ingels@stanford.edu (N.B. Ingels Jr.).

0021-9290/$ - see front matter © 2009 Elsevier Ltd. All rights reserved.
doi:10.1016/j.jbiomech.2009.08.028

1a), 16 around the mitral annulus (Annular Markers, Fig. 1a), 16 on the atrial aspect of the anterior MV leaflet (7 on the MV leaflet edge (#1–7, Fig. 1b); 9 on the leaflet belly (#8–16, Fig. 1b)), and one on the central edge of the middle scallop of the posterior mitral leaflet (PML, Fig. 1a). In the catheterization laboratory, under open-chest conditions, videofluoroscopic images (60 frames/s) of all markers were acquired with the heart in normal sinus rhythm and ventilation transiently arrested at end expiration. Left atrial pressure (LAP), left ventricular pressure (LVP), and aortic pressure (AoP) were continuously measured by catheter-tip manometers. Data were obtained before (CRTL) and after β-blockade with esmolol (ESML, 10–25 mg bolus to achieve ≈15% reduction in LV ESP). Marker coordinates from each view were then merged to yield the 3-D coordinates of the centroid of each marker in each frame, accurate to 0.1 ± 0.3 mm (Daughters et al., 1989; Niczyporuk and Miller, 1991).

Three consecutive beats in sinus rhythm were selected for analysis for both runs (CRTL, ESML) in each heart. For each of these beats, the valve closure time point (t_1) was defined as the frame when the distance between marker #4 on the anterior leaflet and its counterpart on the central posterior leaflet initially fell to a stable minimum (Fig. 1d, lower left red dot) and left ventricular and left atrial pressures at that time were noted (LVP_1, LAP_1). The end IVC time point (t_2, Fig. 1d, upper left red dot) was defined from the AoP deflection and left ventricular and left atrial pressures at that time were noted (LVP_2, LAP_2). The frame during IVR when left ventricular pressure most closely matched LVP_1 (Fig. 1d, lower right blue dot) was defined as t_3 with pressures LVP_3 and LAP_3. The frame during IVR when left ventricular pressure most closely matched LVP_2 (Fig. 1d, upper right blue dot) was defined as t_4 with pressures LVP_4 and LAP_4. Fig. 1d shows leaflet geometry at the t_2 and t_4 matched LVP's for a representative beat in this study.

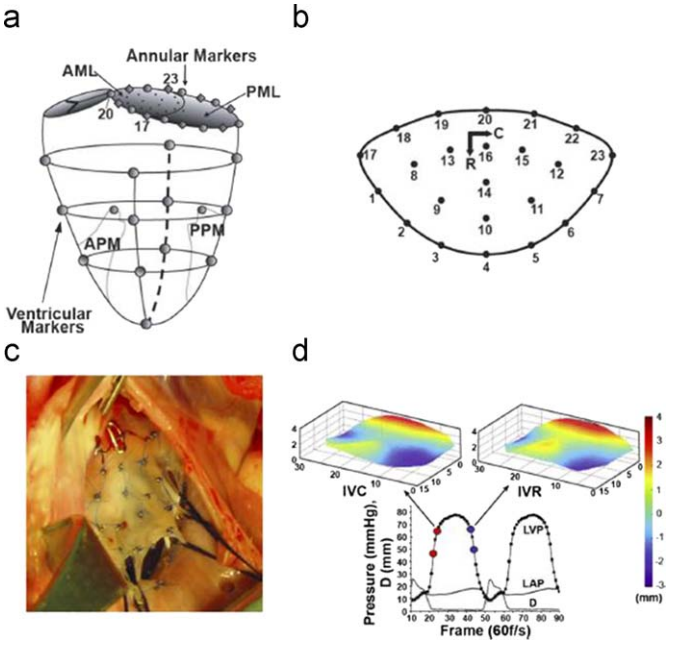

Fig. 1. Marker schematic and pressure depiction.

2.2. Inverse finite element analysis

The inverse finite element analysis methodology to determine the material properties of the anterior mitral valve leaflet has been previously described (Krishnamurthy et al., 2008, 2009; Itoh et al., 2009). These previous studies, however, employed a homogeneous finite element model with two independent material parameters, whereas this current study uses a heterogeneous regional finite element model with six independent material parameters.

2.2.1. Finite element model

Finite element models of the anterior MV leaflet were individually developed for both IVC and IVR intervals for each of the 30 beats analyzed. The geometry of the anterior leaflet was initially defined by the 3-D coordinates of the leaflet markers (Fig. 1b) at t_1 for IVC and t_3 for IVR. Five cubic splines were generated through: (a) Markers 17-1-2-3-4-5-6-7-23; (b) Markers 18-8-9-10-11-12-22; (c) Markers 19-13-14-15-21; (d) Markers 19-16-21; and (e) Markers 19-20-21.

For the purpose of defining the MV leaflet material properties, a coordinate system was defined with the origin at the center of the 16 markers defining the saddle-shaped annulus at t_1 for IVC and t_3 for IVR (Levine et al., 1989). A line from this origin to marker #20 was defined as the leaflet radial axis (*R*, Fig. 1b). The leaflet circumferential axis (*C*, Fig. 1b) was defined normal to *R* and in the plane containing *R* and the posterior commissural marker (#23, Fig. 1b).

The material model of the leaflet was assumed to be orthotropic linear elastic with an a priori assumed Poisson's ratio of 0.49. We have previously demonstrated (Krishnamurthy et al., 2009) that the closed mitral valve had a linear stress strain behavior over physiologic range of pressures and hence we have used a linear elastic model in our analysis. The bi-cubic leaflet surface was divided into three regions with two independent material properties (radial elastic modulus and circumferential elastic modulus) for each region: an ANNULAR region bounded by markers 17-18-19-20-21-22-23-12-15-16-13-8-17; a BELLY region bounded by markers 8-9-10-11-12-15-16-13-8; and an EDGE region bounded by markers 1-2-3-4-5-6-7-22-23-12-11-10-9-8-18-17-1. Two separate shells were used to define the varying thickness of the leaflet regions using data obtained from our histological study of an anterior leaflet from a representative ovine heart. The first shell defined a region from the annulus to 75% of the leaflet towards the free edge; this region had thickness values that varied linearly from 1.2 mm at the annulus to 0.7 mm 75% toward the leaflet free edge. The second shell defined the remaining 25% of the leaflet with a uniform thickness value of 0.2 mm. The bi-cubic surface fit of the MV leaflet was then meshed with 2-D plane-stress quadrilateral shell elements. An element size of 0.004 cm^2 was selected yielding a mesh size of ~2000 elements for a typical anterior leaflet.

The strut chordae were defined as structures undergoing pure tension. A previously published ex vivo modulus (elastic modulus = 20 N/mm^2; cross sectional area = 0.008 cm^2) was used for the strut chordae (Kunzelman and Cochran, 1992). Tension-only bar elements were defined as radiating from the papillary muscle tip marker points (APM and PPM, Fig. 1a) to leaflet belly insertion positions.

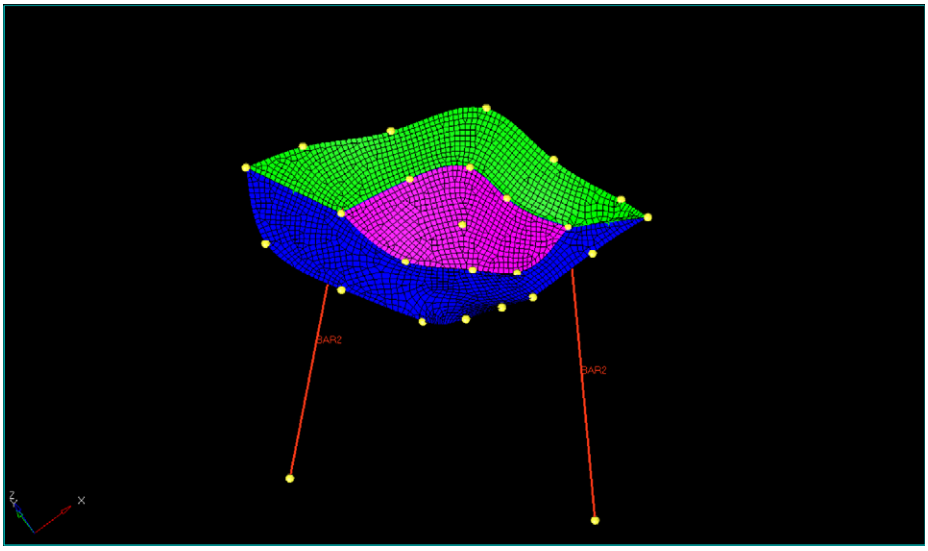

Fig. 2. Heterogeneous FEA model.

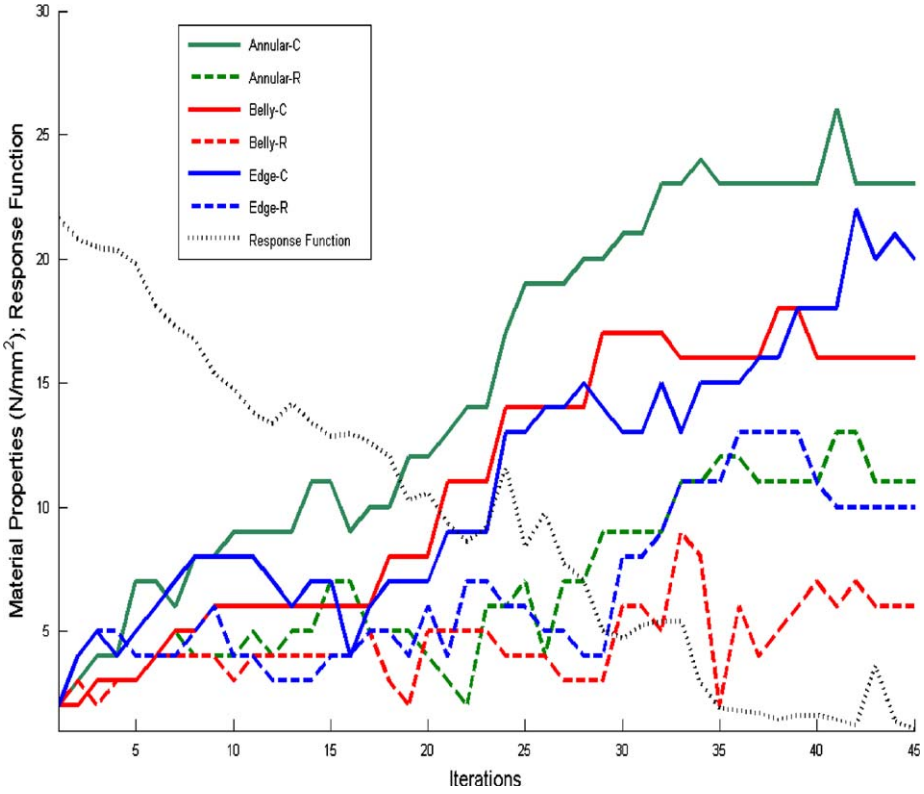

Fig. 3. Material parameter identification process.

The boundary conditions were then enforced on the finite element models. For IVC, (LVP_2–LVP_1) was applied to the ventricular surface of the leaflet and (LAP_2–LAP_1) to the atrial surface. For IVR, (LVP_4–LVP_3) was applied to the ventricular surface and (LAP_4–LAP_3) to the atrial surface. The displacements of the annular markers (#17–23, Fig. 1b), anterior leaflet free-edge markers (#1–7, Fig. 1b) and papillary tip markers (APM and PPM, Fig. 1a) were defined using actual marker data from t_1 to t_2 for IVC and t_3 to t_4 for IVR.

The finite element model (Fig. 2) was then solved for the enforced boundary conditions to obtain the simulated displacements of the leaflet markers.

2.2.2. Inverse finite element analysis algorithm

An inverse finite element analysis then yielded the *in vivo* regional material properties of the leaflet during IVC and IVR. In this algorithm, model-simulated displacements of the leaflet markers were compared with the actual measured displacements of these markers during IVC or IVR to yield a response function defined as the root mean squared (RMS) displacement difference between simulated and actual displacements of the leaflet markers. A parameter identification algorithm (Belegundu et al., 2004), was then used to minimize the response function by repeated iterations of the six independent material properties (Circumferential and Radial Elastic Moduli for ANNULAR, BELLY and EDGE) in each finite element model until a global minimum was obtained (Fig. 3). In our previous study (Itoh et al., 2009) we found that anterior leaflet circumferential–radial shear during IVC and IVR proved sufficiently small that radial and circumferential elastic moduli were unchanged with inclusion or exclusion of this shear modulus in the parameter identification process.

The material property values (Circumferential and Radial Elastic Moduli for ANNULAR, BELLY and EDGE) obtained at the end of the parameter identification runs with the response function at its global minimum were interpreted as the *in vivo* material properties of the anterior MV leaflet during IVC and IVR. That is, these material property values, when used in the finite element model for the anterior leaflet under the enforced pressure and geometric boundary conditions, produced, as closely as possible, the same leaflet marker displacements as those measured experimentally during IVC and IVR. In our previously published study (Krishnamurthy et al., 2008;) we described our extensive analysis, seeding different combinations of radial and circumferential moduli, that demonstrated that the response function minimum and parameters obtained from the analysis were unique.

3. Results

Table 1a shows the mean ($\pm$SD) circumferential elastic moduli for the ANNULAR, BELLY and EDGE regions of the anterior mitral leaflet during IVC and IVR for CTRL and ESML. Table 1b shows the mean ($\pm$SD) radial elastic moduli for the ANNULAR, BELLY and EDGE regions during IVC and IVR for CTRL and ESML. Fig. 4 graphically depicts the mean values from Table 1a and b.

Both circumferential and radial IVC stiffness was 40–58% greater than IVR stiffness for all regions and all CTRL beats. ESML had no effect on IVR stiffness in any region, no effect on EDGE IVC stiffness, but reduced ANNULAR IVC stiffness to ANNULAR IVR stiffness values.

Table 1
Material properties.

	CTRL–IVC	CTRL–IVR	ESML–IVC	ESML–IVR
(a) Circumferential Elastic Moduluselastic modulus (n=10) in N/mm^2				
Annular	68 ± 19	$48 \pm 16^*$	$48 \pm 17^{\#}$	46 ± 16
Belly	54 ± 13	$34 \pm 10^*$	$45 \pm 13^{\#}$	$35 \pm 10^*$
Edge	59 ± 17	$42 \pm 14^*$	57 ± 16	$42 \pm 14^*$
(b) Radial Elastic Moduluselastic modulus (n=10) in N/mm^2				
Annular	26 ± 6	$17 \pm 4^*$	$17 \pm 4^{\#}$	17 ± 4
Belly	19 ± 5	$12 \pm 3^*$	$15 \pm 4^{\#}$	$12 \pm 3^*$
Edge	23 ± 5	$15 \pm 4^*$	22 ± 5	$15 \pm 4^*$

Mean $\pm$ SD of the Circumferential Elastic Moduluscircumferential elastic modulus for the Annular, Belly and Edge regions for CTRL and ESML during IVC and IVR. $p < 0.01$ * IVC versus IVR, # CTRL–IVC versus ESML–IVC from paired t-test.
Mean $\pm$ SD of the Radial Elastic Modulusradial elastic modulus for the Annular, Belly and Edge regions for CTRL and ESML during IVC and IVR. $p < 0.01$ * IVC versus IVR, # CTRL–IVC versus ESML–IVC from paired t-test.

4. Discussion

This study is the first to define regional material properties of the anterior mitral leaflet in the beating heart. The principal findings of this study were: (i) IVC stiffness was greater than IVR

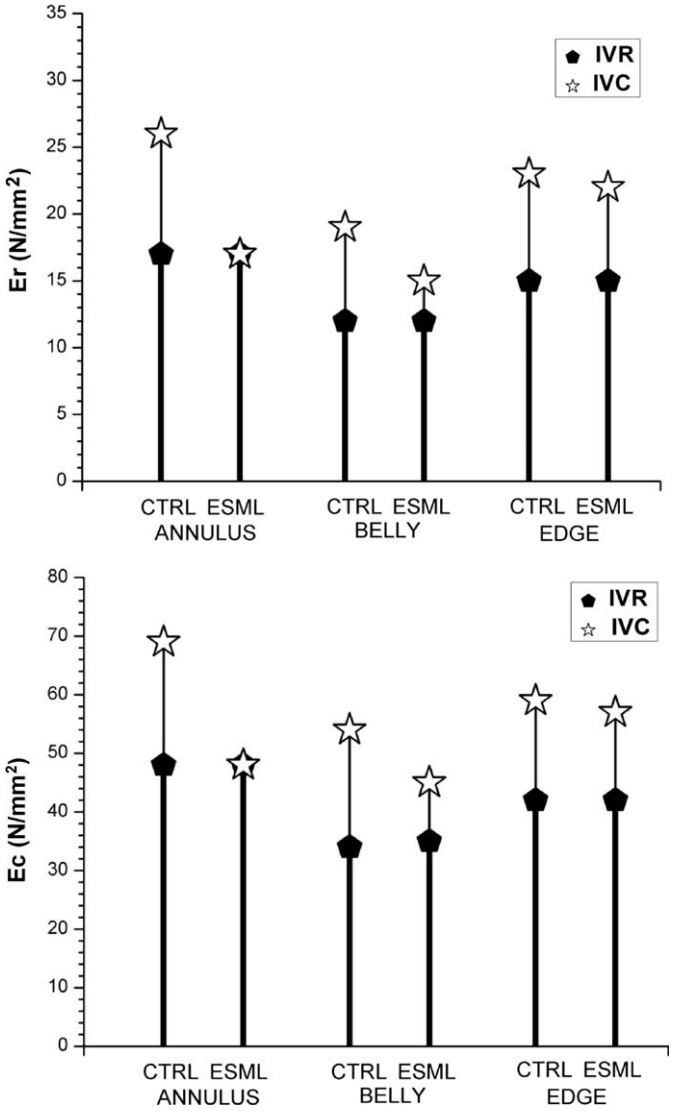

Fig. 4. Material properties.

stiffness in all regions for all CNTRL beats; (ii) β-receptor blockade by esmolol did not affect IVR stiffness in any region; and (iii) ESML selectively reduced ANNULAR IVC stiffness to equal ANNULAR IVR stiffness values. These latter two findings strongly implicate transient tensing of leaflet atrial muscle during IVC as the basis of the ANNULAR IVC–IVR stiffness difference.

An unexpected observation in this study, however, was that the leaflet EDGE region was also stiffer in IVC than IVR, but the stiffness difference in this region was unaffected by ESML β-receptor blockade. Such an IVC–IVR stiffening difference in the EDGE region could not be due to tensing of cardiac muscle, as such muscle does not extend into the EDGE region, but must reflect some other mechanism. One explanation for the EDGE IVC–IVR stiffness difference could be the presence of another contractile mechanism at the EDGE which is insensitive to β-receptor blockade. Another mechanism that could explain this EDGE IVC–IVR stiffness difference is suggested by the data in Fig. 5, displaying the distance between adjacent marker pairs along the central meridian of the leaflet. Note that in the time interval studied during IVC the distance between EDGE markers #4 and #10 is falling, showing a geometric change of this region during this interval. This behavior, found in all 10 hearts, was observed only in the EDGE region of the leaflet, as the distances between markers #10 and #14, #14 and #16 and #16 and #20 remained virtually constant during this portion of IVC when the anterior and posterior leaflets are making final contact. We interpret this as reflecting bending of the anterior leaflet edge, bringing markers #4 and #10 closer together as contact pressure with the posterior leaflet increases during coaptation. This reduction in EDGE radius of curvature would effectively stiffen this region, not by changing its material properties, but simply by changing the geometry of the region to a shape deforming less with a given change in pressure. This could be an important mechanism allowing this specialized region of the leaflet, which needs to be almost negligibly thin and highly flexible to properly coapt with the posterior leaflet and prevent regurgitation, to withstand the sudden very great increase in pressure loading accompanying the onset of each left ventricular systole during IVC. Thus this thin EDGE region may be employing "geometric stiffening" to meet the sudden pressure loading demands during IVC, a mechanism not required by the thicker and more muscular ANNULAR and BELLY

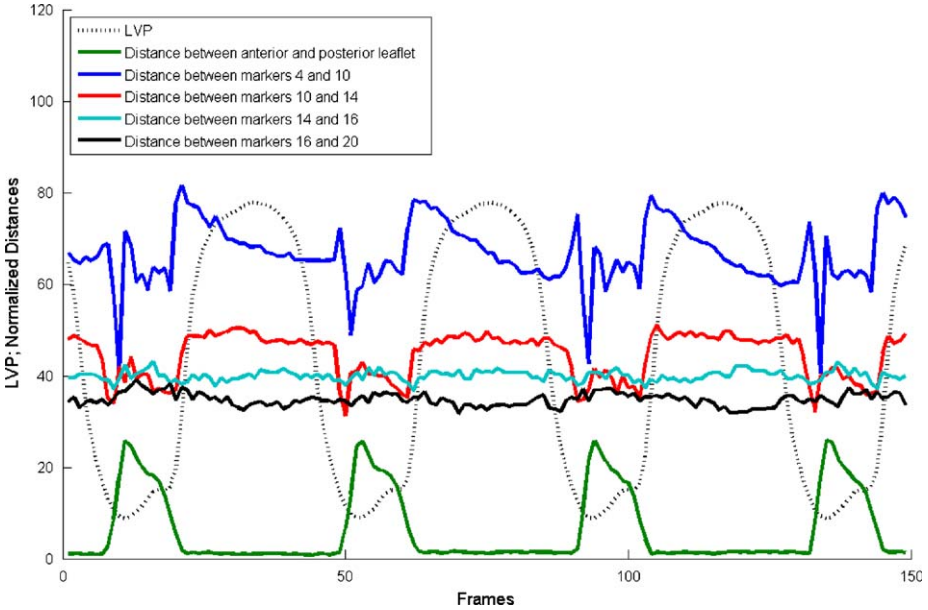

Fig. 5. Temporal changes in leaflet geometry.

regions, whose geometry does not change significantly during IVC or IVR.

Conflict of interest statement

The authors have no conflicts of interest.

Acknowledgments

The authors gratefully acknowledge the expert technical assistance of Sigurd Hartnett, BS, Maggie Brophy, AS, Eleazar Briones, BA, and George T. Daughters, MS.

This study was supported by National Heart, Lung and Blood Institute Grants HL-29589 and HL-67025. Gaurav Krishnamurthy was supported by the BioX Medtronic Graduate Fellowship, Wolfgang Bothe was supported by the Deutsche Herzstiftung, Frankfurt, Germany, and Julia C. Swanson was supported by the Western States Affiliate AHA Postdoctoral Fellowship.

References

Belegundu, A.D., Damle, A., Rajan, S.D., Dattaguru, B.J.a.S.V., 2004. Parallel line search in method of feasible directions. Optim. Eng. 5, 379–388.

Boucek, R.J., Bouckova, B., Levy, S., 1978. Anatomical arrangement of muscle tissue in the anterior mitral leaflet in man. Cardiovasc. Res. 12 (11), 675–680.

Cooper, T., Napolitano, L.M., Fitzgerald, M.J., Moore, K.E., Daggett, W.M., Willman, V.L., Sonnenblick, E.H., Hanlon, C.R., 1966. Structural basis of cardiac valvar function. Arch. Surg. 93 (5), 767–771.

Daughters, G.T., Sanders, W.J., Miller, D.C., Schwarzkopf, A., Mead, C.W., Ingels, N.B.J., 1989. A comparison of two analytical systems for 3-D reconstruction from biplane videoradiograms. IEEE Comput. Cardiol. 15, 79–82.

Fenoglio Jr., J.J., Tuan Duc, P., Wit, A.L., Bassett, A.L., Wagner, B.M., 1972. Canine mitral complex. Ultrastructure and electromechanical properties. Circ. Res. 31 (3), 417–430.

Hibbs, R.G., Ellison, J.P., 1973. The atrioventricular valves of the guinea-pig, II. An ultrastructural study. Am. J. Anat. 138 (3), 347–369.

Itoh, A., Krishnamurthy, G., Swanson, J.C., Ennis, D.B., Bothe, W., Kuhl, E., Karlsson, M., Davis, L.R., Miller, D.C., Ingels Jr., N.B., 2009. Active stiffening of mitral valve leaflets in the beating heart. Am. J. Physiol. Heart Circ. Physiol. .

Krishnamurthy, G., Ennis, D.B., Itoh, A., Bothe, W., Swanson, J.C., Karlsson, M., Kuhl, E., Miller, D.C., Ingels Jr., N.B., 2008. Material properties of the ovine mitral valve anterior leaflet in vivo from inverse finite element analysis. Am. J. Physiol. Heart Circ. Physiol. 295 (3), H1141–H1149.

Krishnamurthy, G., Itoh, A., Bothe, W., Swanson, J.C., Kuhl, E., Karlsson, M., Miller, D.C., Ingels Jr., N.B., 2009. Stress–strain behavior of mitral valve leaflets in the beating ovine heart. J. Biomech. .

Kunzelman, K.S., Cochran, R.P., 1992. Stress/strain characteristics of porcine mitral valve tissue: parallel versus perpendicular collagen orientation. J. Card. Surg. 7 (1), 71–78.

Levine, R.A., Handschumacher, M.D., Sanfilippo, A.J., Hagege, A.A., Harrigan, P., Marshall, J.E., Weyman, A.E., 1989. Three-dimensional echocardiographic reconstruction of the mitral valve, with implications for the diagnosis of mitral valve prolapse. Circulation 80 (3), 589–598.

Montiel, M.M., 1970. Muscular apparatus of the mitral valve in man and its involvement in left-sided cardiac hypertrophy. Am. J. Cardiol. 26 (4), 341–344.

Niczyporuk, M.A., Miller, D.C., 1991. Automatic tracking and digitization of multiple radiopaque myocardial markers. Comput. Biomed. Res. 24 (2), 129–142.

Wit, A.L., Fenoglio Jr., J.J., Hordof, A.J., Reemtsma, K., 1979. Ultrastructure and transmembrane potentials of cardiac muscle in the human anterior mitral valve leaflet. Circulation 59 (6), 1284–1292.

Wit, A.L., Fenoglio Jr., J.J., Wagner, B.M., Bassett, A.L., 1973. Electrophysiological properties of cardiac muscle in the anterior mitral valve leaflet and the adjacent atrium in the dog. Possible implications for the genesis of atrial dysrhythmias. Circ. Res. 32 (6), 731–745.